ADVANCED MATERIALS INTERFACES
www.advmatinterfaces.de

Trapped Air-Induced Reversible Transition between Underwater Superaerophilicity and Superaerophobicity on the Femtosecond Laser-Ablated Superhydrophobic PTFE Surfaces

Jinglan Huo, Jiale Yong, Feng Chen,* Qing Yang, Yao Fang, and Xun Hou*

Controlling the behavior of underwater bubbles on a solid surface and establishing the contact model between a gas bubble and a solid substrate in a water medium have great significance. Herein, a method is proposed to realize the reversible switching between underwater superaerophilicity and superaerophobicity on the femtosecond laser-induced rough polytetrafluoroethylene (PTFE) surface by controlling the trapped air layer in water. The original femtosecond laser-structured PTFE surface is superhydrophobic in air and superaerophilic in water. After vacuum-pumping treatment, the trapped air layer around the microstructures of the underwater superhydrophobic PTFE surface is removed, leading to the underwater superaerophobicity of the sample surface. The trapped air layer can be recovered and the PTFE surface can regain the underwater superaerophilicity by drying treatment and the immersion of the sample in water again. Such a round-trip transition can achieve the bubble's "locating capture" and the control of the selective passage of air bubbles through a perforated rough PTFE sheet. It is believed that the resultant underwater superaerophobic and superaerophilic surfaces will have significant applications in manufacturing submarine gas-collection devices, improving the chemical reaction between liquid reagent and gas, and avoiding the microchannel blockage caused by bubbles in microfluidics and biosensor devices.

1. Introduction

The behavior of gas bubbles on a solid substrate in aqueous medium has been emerged as a new research focus recently owing to its wide application prospects.[1–8] The attachment and detachment of underwater bubbles on a substrate are relevant to our lives, or even industrial and military fields.[9–14] For instance, diving bugs and beetles can submerge into water for a long time due to the existence of physical gills to store enough O_2 underwater.[15] The attachment of air bubbles on the mineral ores contributes to increasing the efficiency of froth floatation process.[16] The absorption of air bubbles on the submarine vessels is perceived as a suitable approach for drag reduction.[17] The timely removal of bubbles in a microfluidic system can prevent the bubbles from blocking the microchannels.[18] The adhesion of the generated gas bubbles on the electrode usually results in a remarkable decline of reaction rate in an electrochemical reaction.[3] Such problem can be prevented by allowing the bubbles to timely detach from the electrode surface. Until now, two superwetting states related to the underwater bubble's behavior at the liquid/solid/gas interface have been mostly investigated because of their corresponding performances in gas-repellency and gas-absorption, known as the underwater superaerophobicity and superaerophilicity, respectively.[19–29] Jiang et al. found the burst and capture effect of air bubbles coming in contact with a superhydrophobic lotus leaf surface in water.[19] They also fabricated an artificial superhydrophobic silicon surface that reproduced the hierarchical rough surface microstructures of a lotus leaf and also achieved gas-absorption by using the as-prepared surface. Yong et al. revealed the relationship between the extreme wettability of water droplet in air and the opposite behavior of air bubble in water on a textured solid substrate inspired by lotus leaf and fish scale.[20] The biomimetic superhydrophobic polydimethylsiloxane (PDMS) surface and superhydrophilic silicon surface were structured by femtosecond laser ablation, and showed underwater superaerophilicity and superaerophobicity, respectively. Feng et al. reported an underwater superaerophilic oxygen-rich enzyme biosensor based on the superhydrophobic Pt-catalyst-modified carbon-fiber mesh.[23] After immersing the superaerophilic electrode into analyte solution, the oxygen supply from the captured air cushion was sufficient and the oxygen diffusion was particularly high for accurate analyte levels determination. Lu et al. fabricated a kind of underwater superaerophobic MoS_2 nanostructured film contained vertically aligned MoS_2 nanoplatelets.[3] By using such film as an

Dr. J. Huo, Dr. J. Yong, Prof. F. Chen, Dr. Y. Fang, Prof. X. Hou
State Key Laboratory for Manufacturing System Engineering and Shaanxi Key Laboratory of Photonics Technology for Information
School of Electronics & Information Engineering
Xi'an Jiaotong University
Xi'an 710049, P. R. China
E-mail: jlyong@xjtu.edu.cn; chenfeng@mail.xjtu.edu.cn
Prof. Q. Yang
School of Mechanical Engineering
Xi'an Jiaotong University
Xi'an 710049, P. R. China
The ORCID identification number(s) for the author(s) of this article can be found under https://doi.org/10.1002/admi.201900262.

DOI: 10.1002/admi.201900262

electrode, the adhesion of generated H_2 bubbles on the electrode was effectively avoided in hydrogen evolution reaction. The in-time leaving of the bubbles greatly improved the electrocatalytic performance. Yong et al. designed different water/bubbles separation devices by using the superhydrophobic/superaerophilic or the superhydrophilic/superaerophobic nanoneedle-coated copper mesh as the core components.[22] Although a large number of superwetting surfaces with the ability of gas-repellency or gas-absorption, respectively, have been fabricated by different microfabrication methods, the integration of those two opposite functions on a same surface—that is, a smart surface can reversibly switch its underwater bubble's wettability between underwater superaerophobicity and superaerophilicity—has great significances but has rarely been reported until now.[30–33] In addition, the influence factor and theoretical analysis of underwater superaerophobicity and underwater superaerophilicity still wait to be studied to understand how to control the behavior of in-water bubbles.

In this paper, we indicated that the trapped air layer between water and the immersed structured substrate was the key factor of controlling the underwater bubbles' behavior on a solid surface, which was verified through manipulating the existence of trapped air layer or not on the femtosecond laser-induced rough polytetrafluoroethylene (PTFE) surface. The original textured PTFE surface exhibited superhydrophobicity in air and superaerophilicity in water. However, after vacuum-pumping treatment in water, the sample switched to be underwater superaerophobic as the trapped air layer was removed. After being dried off in a drying oven, the original underwater superaerophilic property of the structured PTFE surface could be recovered. The transition between the two superwettabilities to an underwater air bubble could be reversibly switched by alternate vacuum-pumping and drying treatments for many times. In addition, by controlling of the trapped air layer, the bubble "locating capture" and the selective passage of bubbles were also realized.

2. Results and Discussion

The femtosecond laser microfabrication system for preparing original superhydrophobic PTFE surface was shown in **Figure 1**a. The laser pulses were focused on the sample surface through an objective lens and ablated the surface via using a "line-by-line" scanning process. The subsequent vacuuming treatment and measurement process of the behavior of bubbles on the surface were depicted in Figure 1b,c.

Figure 2a–c shows the scanning electronic microscopy (SEM) images of the PTFE surface after femtosecond laser ablation. The structured surface presents a coral-forest-like morphology consisting of plenty of microscale protrusions and pores with both diameters of 1–2.5 µm (Figure 2a,b). The surface of the protrusions is further decorated with a large number of nanoscale fine protuberances (Figure 2c). The size of those nanostructures ranges from 200 to 500 nm. This kind of dual-scale microstructures is caused by the instantaneous melt and the resolidification of ejected PTFE during the femtosecond laser ablation.[34–36]

Laser-induced microstructure endows the surface with adequate roughness, which has great enhancement for the surface wettability of the intrinsically hydrophobic PTFE to superhydrophobicity.[34–38] A 7 µL water droplet on the as-prepared surface presented a spherical shape with the water contact angle (WCA) of 154° (Figure 2d). When the surface was tilted to only 5°, the water droplet could roll down easily (inset of Figure 2d). Such low water sliding angle (WSA) of 5° indicates that the laser-induced rough surface showed superhydrophobicity and ultralow adhesion to a water droplet. The water droplet on the rough PTFE surface was at the Cassie wetting state in which the droplet could only touches the top part of the rough microstructures. It was the existence of a trapped air layer between the surface microstructure and the water droplet that impeded the effective contact between the droplet and the laser-induced microstructure.

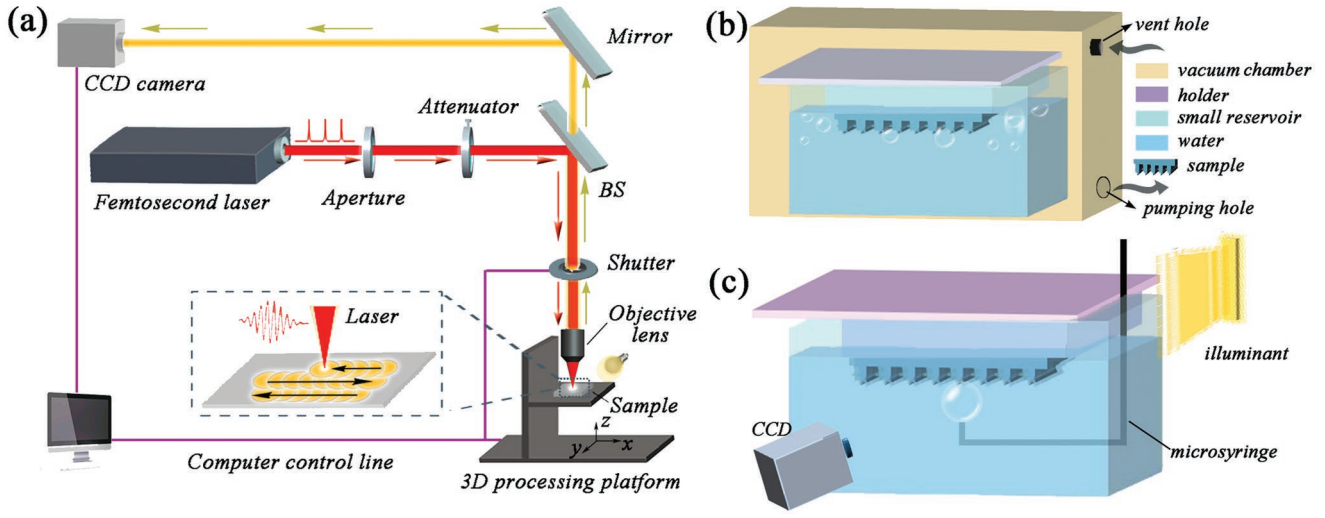

Figure 1. Schematic diagrams of a) the femtosecond laser microfabrication system, b) the experimental setup for vacuum-pumping treatment in water, and c) the underwater bubble contact angle measurement.

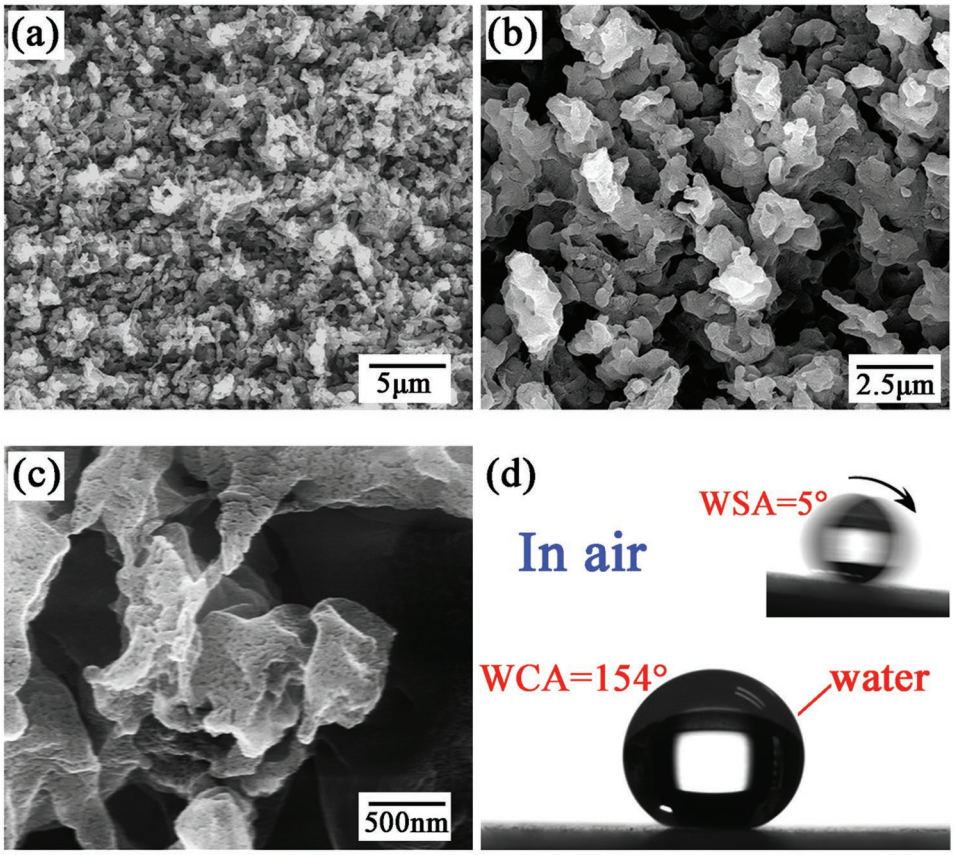

Figure 2. Surface microstructure and superhydrophobicity of the PTFE surface after femtosecond laser ablation. a–c) SEM images of the treated PTFE surface at different magnification. d) Shape of a water droplet on the rough PTFE surface in air. The inset shows that a water droplet can easily roll off a 5° tilted rough PTFE surface.

The underwater bubble wettability was investigated by the immersion of the as-prepared superhydrophobic PTFE sample in water with its processing side facing down (Figure 1c). **Figure 3**a shows the static behavior of a bubble on the rough PTFE surface in a water medium. When an air bubble was released below, the bubble would rise upward driven by buoyancy. Once touching the sample surface, the bubble would burst, spread out, and merge with the prior-existing air cushion over the microstructures within 0.12 s (Figure 3c). The measured bubble contact angle (BCA) was as low as 8.5°, revealing that the laser-induced superhydrophobic PTFE surface showed superaerophilicity in water (Figure 3a).

Interestingly, the wettability of the bubble on the as-prepared surface could be switched from underwater superaerophilicity to superaerophobicity just through simple vacuum-pumping treatment (Figure 1b). Before the vacuum-pumping treatment, it is proved that there existed an in-water trapped air cushion on the as-prepared PTFE. A silver-mirror-like reflectance (**Figure 4**a,c) appeared on the laser-treated surface when the sample was dipped into water. An inward wetting meniscus (Figure 4c) at water/air interface could also be observed when the sample was vertically inserted in water. With the decrease of the pressure in the chamber, the pressure difference between the trapped air cushion and ambient pressure occurred and got larger gradually. Driven by the Laplace pressure of the trapped air cushion, equilibrium state of the water/air interface was broken, and the extrusion of air among the microstructures happened. Decreasing the ambient pressure successively until nearly no air bubbles escaped from the sample surface, there was scarcely any air retaining in the rough microstructures. As a result, the space of the original trapped air layer was replaced by water and the rough surface microstructure was thoroughly "wetted" by water. It could be confirmed by the disappearance of the underwater silver-mirror-like reflectance on the sample surface (Figure 4b,d) and an outward wetting meniscus at the water/air interface of the vertically inserted PTFE sheet (Figure 4d). At this moment, the laser-induced rough PTFE surface could be regarded to become "superhydrophilic" in water although it was still superhydrophobic in air. When a bubble was placed onto the PTFE surface with keeping the PTFE sheet in water, the BCA of the bubble was measured to be 157.5°, demonstrating that the same femtosecond laser-induced rough PTFE surface turned to be superaerophobic after vacuum-pumping treatment (Figure 3b). Figure 3d shows the process of an air bubble rolling up along the sample surface with the tilted angle of only 5°, which indicates the underwater superaerophobic sample surface owning an ultralow adhesion to the bubbles. After being taken out of water and dried off in a drying stove at 60 °C for 1 h, the rough PTFE surface could recover its in-air superhydrophobicity and underwater superaerophilicity

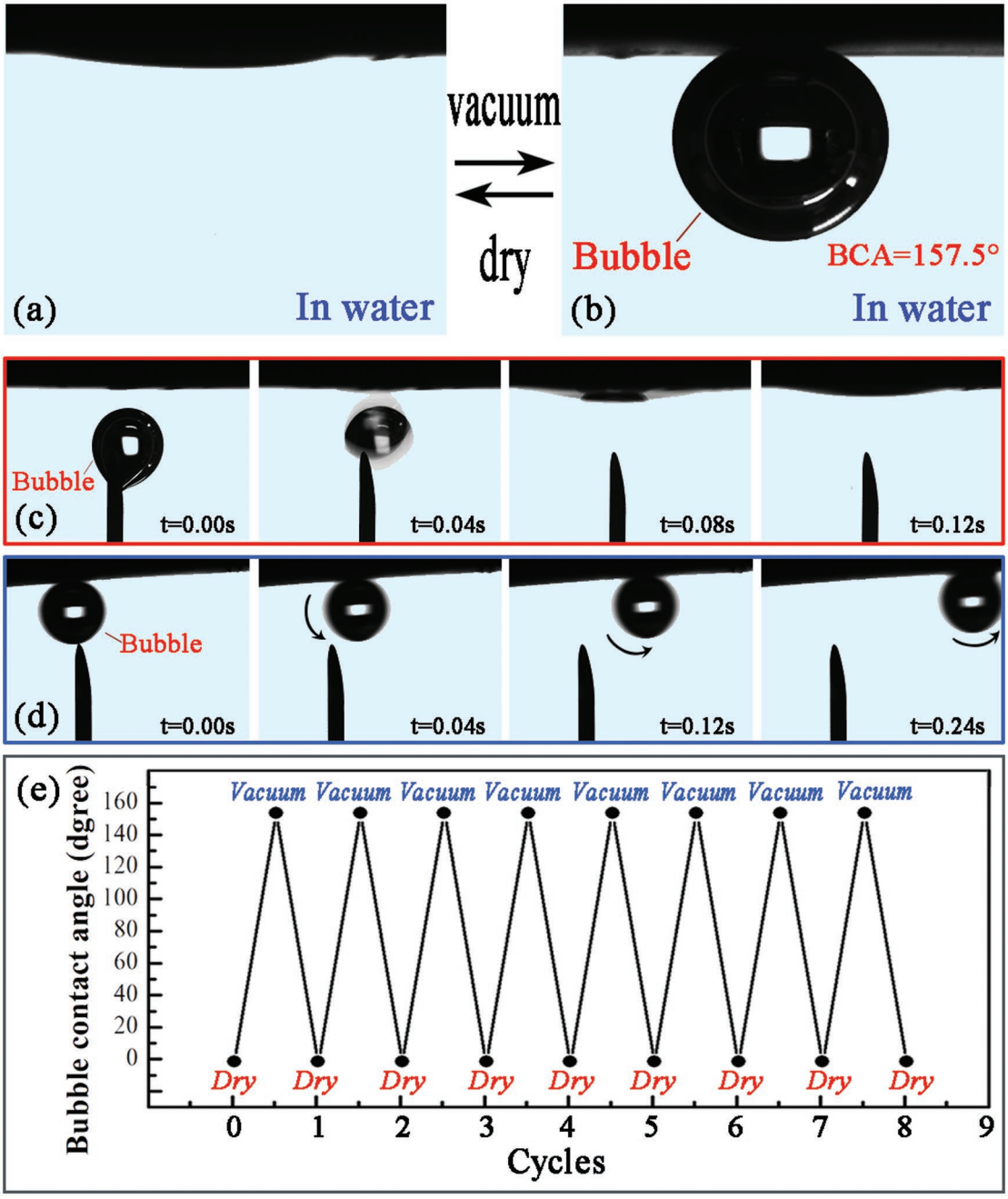

Figure 3. Reversible switching between underwater superaerophilicity and superaerophobicity on the femtosecond laser ablated PTFE surface by alternate vacuuming and drying treatments. Images of an underwater bubble on the as-prepared surface after being a) dried for 1 h and b) vacuumized in water, respectively. c) Time sequence of the dynamic spreading process of a bubble toward the original superhydrophobic PTFE surface in water. d) Process of an underwater bubble rolling on the 5° tilted surface after vacuum-pumping treatment. e) The reversible and repeatable switching between the underwater superaerophilicity and superaerophobicity.

(Figure 3a). The reversible transition between underwater superaerophilicity and superaerophobicity could be cycled for many times (Figure 3e).

Figure 5 shows the underlying mechanism and theoretical evaluation of the reversible switch between underwater superaerophobicity and superaerophilicity on the rough PTFE surface. The PTFE surface was endowed with hierarchical micro- and nanoscale structures by femtosecond laser ablation. With the synergistic effect of the intrinsic hydrophobicity of PTFE substrate and the laser-induced rough microstructure, the resultant surface was not unexpected to exhibit superhydrophobicity in air, like the superhydrophobicity of lotus leaf. After the immersion of the PTFE sheet in water and the formation of the well-stabilized trapped air layer, water was isolated from

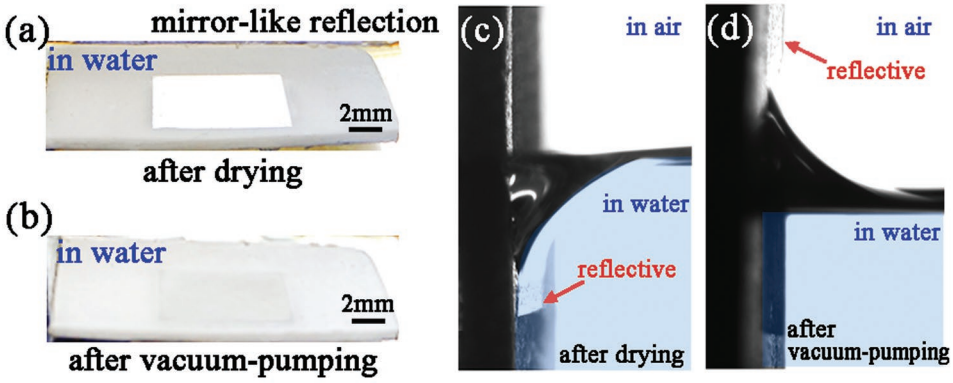

Figure 4. Photographs of the PTFE surfaces in water and the wetting meniscus formation on the vertical as-prepared PTFE surfaces at the water/air surface. a) Underwater silver-mirror-like reflectance on the structured surface after drying. b) No observation of the silver mirror-like reflectance on the structured surface after vacuum-pumping treatment. c) An inward wetting meniscus at the water/air surface after drying. d) An outward wetting meniscus at the water/air surface after vacuum-pumping treatment.

the sample surface by the trapped air and could only touch the peaks of microstructures (Figure 5a). Once a rising bubble was in contacted with the solid–vapor interface, it broke up and the gas in the bubble spread out quickly merging with the original air layer under water pressure (Figure 5b,c). The contact state between the bubble and the PTFE surface could be considered as the Wenzel wetting state in the liquid/solid/vapor three phase system. It was noticeable that the interface of water and the captured gas reached to a state of equilibrium and force balance. According to Laplace equation,[39] the pressure balance of liquid/vapor interface underwater at equilibrium state can be deduced as

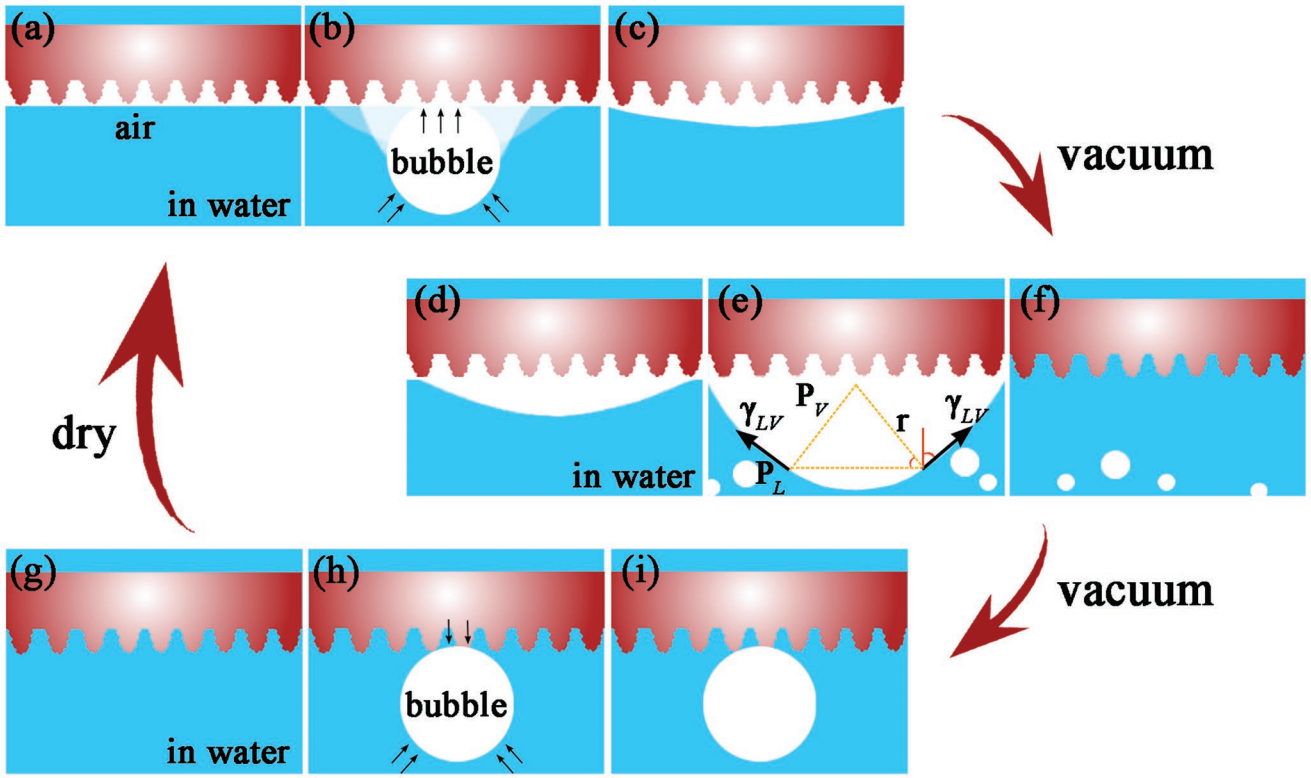

Figure 5. Mechanism of the reversible switching between underwater superaerophobicity and superaerophilicity on the as-prepared superhydrophobic PTFE surface. a–c) Process of a released air bubble merging with existing trapped air in the superhydrophobic rough surface underwater after being dried beforehand. d–f) Process of ejectment of trapped air with vacuumizing sample surface underwater. g–i) Behavior of an air bubble on the superhydrophilic rough surface overtime after vacuum-pumping.

$$P_V - P_0 - P_L = \frac{2\gamma_{LV}}{r} \quad (1)$$

where P_V is the pressure of the trapped air among surface microstructures, P_0 is the ambient gas pressure, P_L is the water pressure correlated with the depth from atmospheric water surface, γ_{LV} is the interfacial free energy between the liquid–vapor, r is the curvature radius of liquid/vapor curve interface (Figure 5e). The pressure difference, ΔP, between P_0 and P_V can be deduced from Equation (1)

$$\Delta P = P_V - P_0 = P_L + \frac{2\gamma_{LV}}{r} \quad (2)$$

It is obvious that the change of ΔP directly influences the r. During the vacuum-pumping process, the P_0 consistently fall, giving rise to an increasing ΔP and a decrease of r. Hence, the trapped air broke away from the microstructures gradually and further effused from water in the form of bubbles. The original air space was replaced by water below (Figure 5d–f). Water entered into the rough structures of the PTFE surface and wetted the surface completely, which resulted that the sample surface was considered to be "superhydrophilic" underwater and became a water/solid composite interface (Figure 5g). While a rising bubble touched the surface, it was inclined to keep a spherical shape on the resultant surface. The reason here is very similar to that of the antiwater property of superhydrophobic surface in air. On the one hand, the water layer trapped around the microstructures impeded the efficient contact between the bubble and inner structures, which caused that the bubble could only touch the apex area of nanoscale protuberances of the sample surface. On the other hand, the trapped water layer owned the inherent repellence to air bubble. It revealed that the contact state of the bubble and the PTFE surface could be equivalent to underwater Cassie state in the liquid/solid/vapor three phase system (Figure 5h). The bubble's spherical shape could maintain overtime (Figure 5i).

When a bubble is placed on the PTFE surface in water, the Gibbs free energy of this system can be expressed as[40]

$$G = \gamma_{LV} S_{LV} + \gamma_{SL} S_{SL} + \gamma_{SV} S_{SV} \quad (3)$$

where γ_{SL} and γ_{SV} represent the interfacial free energy between the solid–liquid and solid–vapor interfaces, respectively. S_{LV}, S_{SL}, and S_{SV} represent the interfacial area between the liquid–vapor, solid–liquid, and solid–vapor interfaces, respectively. There exists the below geometrical relationship

$$S_{LV} = 2\pi R^2 (1 - \cos\theta_V) + (1 - f_{SV})\pi R^2 \sin^2\theta_V$$

$$S_{SV} = \pi R^2 r_V f_{SV} \sin^2\theta_V$$

$$S_{SL} = S_{tot} - \pi R^2 r_V f_{SV} \sin^2\theta_V$$

where R is the radius of the bubble. S_{tot} is the area of the whole rough surface. θ_V is the BCA on liquid/solid compound surface. f_{SV} is the area fraction of the solid part in the compound interface composed of liquid and solid in the bubble-solid contact area, and r_V is the roughness ratio of the part of bubble–solid contact area. In general, the roughness ratio is defined as the ratio of the true surface area to its projected area.

For a bubble with constant volume, V, the R and V have a relationship as

$$R^2 = \left(\frac{3V}{\pi}\right)^{2/3} \left(2 - 3\cos\theta_V + \cos^3\theta_V\right)^{-2/3} \quad (4)$$

The dimensionless Gibbs energy can be expressed as[40]

$$G^* \equiv \frac{G}{\gamma_{LV}\pi^{1/3}(3V)^{2/3}} = (2 - 3\cos\theta_V + \cos^3\theta_V)^{-2/3} \times [2 - 2\cos\theta_V - (r_V f_{SV}\cos\theta_{SV} + f_{SV} - 1)\sin^2\theta_V] \quad (5)$$

where $\cos\theta_{SV} = \frac{\gamma_{SL} - \gamma_{SV}}{\gamma_{LV}}$, θ_{SV} is the intrinsic BCA (Young's BCA) on a flat PTFE surface underwater. Assuming r_V and f_{SV} are the constant values. When $\frac{\partial G^*}{\partial \theta_V} = 0$, the Gibbs free energy takes the minimum, the system is stable

$$\cos\theta_V = r_V f_{SV}\cos\theta_{SV} + f_{SV} - 1 \quad (6)$$

Equation (6) could be regarded as the underwater vision of Cassie equation on liquid/solid compound surface. For the θ_{SV} and θ_V being measured to be 82° and 157.5°, respectively, the maximum value of f_{SV} was calculated as 6.68% ($r_V \geq 1$), indicating a tiny contact between a bubble and the femtosecond laser-induced rough PTFE surface wetted thoroughly underwater.

After the PTFE surface being dried, there is no residual moisture among interspaces of the surface microstructures. A trapped air layer will be formed again once the sample surface was dipped into water again. The PTFE sheet recovered underwater superaerophilicity as well as the capability of capturing and absorbing air bubble underwater. As a result, the reversible switching between underwater superaerophobicity and superaerophilicity on the femtosecond laser-structured PTFE rough surface was realized simply by pumping trapped-gas out in water and in-air drying treatment.

Previously, our group reported an ethanol-assisted prewetting method to turn the laser-structured superhydrophobic Al surface from underwater (super-) aerophilic to superaerophobic.[28] The original superhydrophobic Al surface exhibits (super-) aerophilicity in water, while the surface shows superaerophobicity when it is prewetted with ethanol and then dipped into water. Complete wetting of the superhydrophobic surface microstructure plays a crucial role in the achievement of reversible switching between underwater aerophilicity and superaerophobicity through the ethanol-prewetting method. However, some superhydrophobic surfaces also have the great ability to repel ethanol; that is, such materials are difficult to be wetted by ethanol. Therefore, the ethanol-prewetting method can only allow limited superhydrophobic materials to switch from underwater superaerophilicity to superaerophobicity. Regarding the vacuuming/drying method in this paper, because almost all of the textured materials can be fully "wetted" by water after vacuuming treatment in a water medium, so this

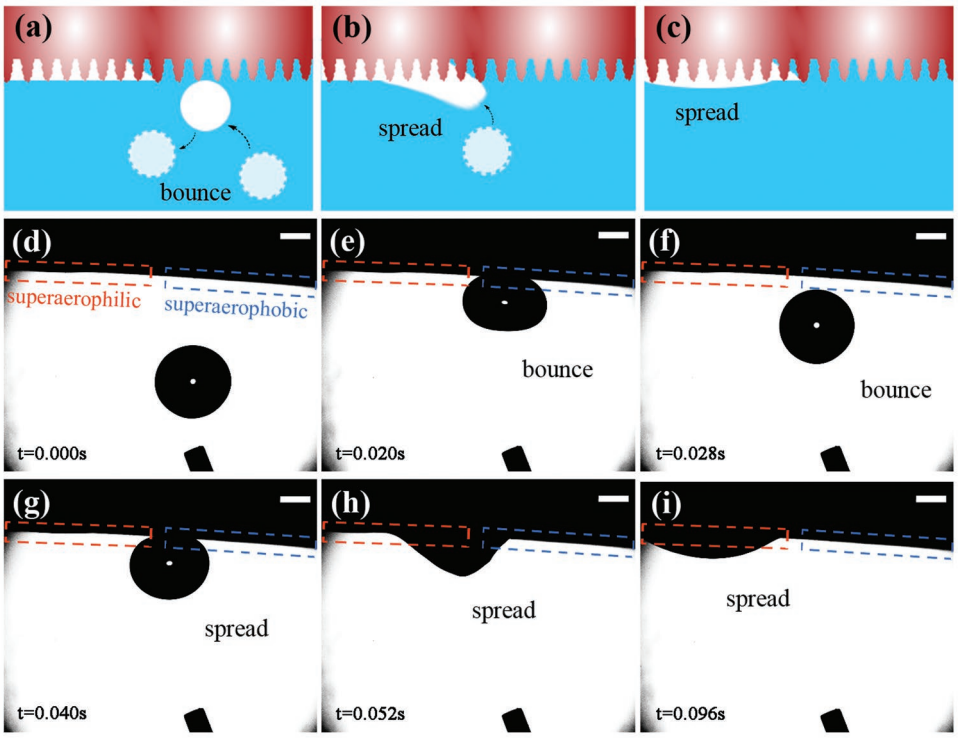

Figure 6. Locating capture of air bubbles by underwater superaerophilic/superaerophobic hybrid surface. a–c) Schematic illustration of the capturing process. d–i) Snapshots process of capturing a released bubble by the hybrid surface. Left part of the sample surface (marked by red dashed box) is underwater superaerophilic, while right part of the sample surface (marked by blue dashed box) is underwater superaerophobic. Scale bars in (d)–(i) are 1 mm.

method can potentially achieve switchable underwater superaerophilicity/superaerophobicity on a wide range of superhydrophobic surfaces.

A bubble "locating capture" device was fabricated by selectively vacuum-treating the rough PTFE surface. The textured PTFE sheet was mounted in a small water reservoir vertically, with half of the laser-structured surface being penetrated into water and another half exposing to air above water surface. The fabricating manner and parameters for treating the PTFE surface are the same as the above-mentioned. Then, the whole setup was moved into vacuum chamber. After vacuum-pumping, the microstructures of the in-water half rough surface were wetted by water and this half was endowed with underwater superaerophobicity. On the contrary, the half in air still maintained the original superhydrophobicity and underwater superaerophilicity. Once the whole PTFE surface was immersed into water, a half of the surface could capture a layer of air to exhibit the superaerophilicity, while another half was wetted by water to exhibit the superaerophobicity. As shown in the schematic illustration images (**Figure 6**a–c), a bubble could bounce on the underwater superaerophobic part while spread out on the underwater superaerophilic part. Figure 6d–i shows the monitored experimental process of "locating capture" of an air bubble on such "half-half" surface tilted at 3° in water. When a released bubble rapidly contacted with the underwater superaerophobic area, it deformed, extruded the surface and then bounced upward because this area hindered the spread and absorption of the bubble (Figure 6d–f). As the bubble bounced to the middle boundary of these two different superwetting areas, the bubble would be absorbed by the superaerophilic surface and spread out on the underwater superaerophilic part (Figure 6g–i). The "locating capture" of bubble was realized by the combination of the femtosecond laser-induced rough microstructures and selective vacuum-pumping treatment.

The switchable transition between underwater superaerophilicity and underwater superaerophobicity on the laser-structured superhydrophobic PTFE surface could be utilized to selectively achieve "bubble passing through" and "bubble interception" on a same porous sheet. A PTFE sheet with thickness of 0.3 mm was first drilled by a mini drill to generate a through-microhole array. Next, hierarchical micro- and nanoscale structures were created on both sides of the porous PTFE sheets by femtosecond laser ablation under the parameters in accordance with the sample before. **Figure 7**a shows the SEM images of the porous textured PTFE surface with different magnification. The diameter of each hole was about 266 μm. It is obvious that the marginal area of a hole also exhibits a rough morphology. After being immersed in water, both sides of the porous rough PTFE surface captured a layer of air cushion. As shown in Figure 7b, once several air bubbles touched the underside, they were absorbed quickly by bottom side of the sheet and merged with the old air cushion on bottom sides as well as the top side because of the microholes letting through those air bubbles. With the increase of the number of bubbles, an elliptical air balloon formed overlaying the surface on account of the intercommunication

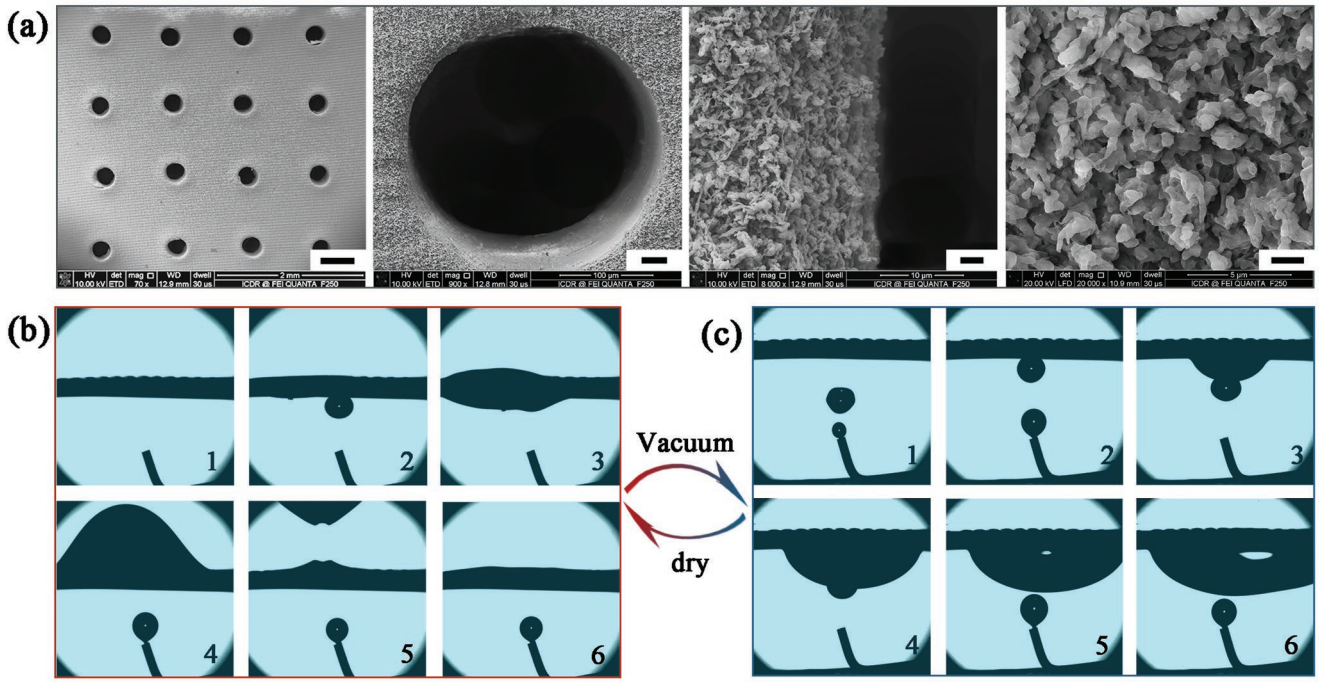

Figure 7. Selective passage of underwater bubbles by using superhydrophobic porous PTFE sheet. a) SEM images of a porous rough PTFE surface with through-microholes array and surrounding laser-induced micro- and nanoscale structures. b) Process of a large amount of underwater bubbles spreading out and then passing through the porous rough PTFE sheet after drying in air. c) Interception of released underwater bubbles below the porous rough PTFE sheet after vacuum-pumping underwater. Scale bars in (a) are 500, 30, 3, and 2 μm.

of holes and water pressure. Continuing to add bubbles, to a certain extent, the air balloon was pulled up by the strong buoyancy, and then left away from the PTFE sheet in the form of a larger bubble. After vacuum-pumping treatment in water, both the microstructures and microholes were wetted by water, hence the sample surface was transferred to be underwater superaerophobic. As shown in Figure 7c, the first released bubble could maintain a spherical shape on the bottom surface of the porous sheet. Then, the next bubbles contacted and merged with the first bubble to expand the volume of the bubble. In spite of the enlargement of bubble volume and buoyancy, the bubble was still intercepted and could not pass through the surface because of the bubble repellency of the superaerophobic microstructures. Identically, after being dried thoroughly, the porous sheet recovered its underwater superaerophilicity and allowed the bubbles to pass through again in a water medium. The passage "turning-on" and "turning-off" properties for bubbles on the same superhydrophobic porous PTFE surface might find wide application in microfluidic devices.

3. Conclusions

In conclusion, a smart rough PTFE surface with switchable underwater bubble's wettability was fabricated by one-step femtosecond laser ablation. The combination of the intrinsic hydrophobicity of PTFE and the laser-induced micro/nanoscale hierarchical structures resulted in the superhydrophobicity of the as-prepared surface in air. Such superhydrophobic surface showed superaerophilicity in water with the ability of absorbing underwater bubbles. Interestingly, the sample could be transformed from superaerophilic to superaerophobic in a water medium by vacuum-pumping treatment. After drying in air, the superhydrophobicity as well as the underwater superaerophilicity of the original femtosecond laser ablated PTFE surface could easily be recovered. It was found that the trapped air layer among the surface microstructure of the PTFE sample played an important role in the transformation between the underwater superaerophilicity and superaerophobicity. The trapped air layer around the superhydrophobic PTFE surface allowed the sample to absorb bubbles in water by merging with the trapped air layer. The vacuum-pumping treatment could remove this trapped air layer and resulted in that the space in the surface microstructure was fully filled with water, endowing the surface with excellent bubble-repellent ability in water. Once the sample was dried and immersed in water again, the trapped air layer was regained, as well as the underwater superaerophilicity. By the means of alternate vacuum-pumping treatment (removing the trapped air layer) and drying treatment (reforming the trapped air layer), the reversible switching between underwater superaerophilicity and superaerophobicity could be cycled for many times. The bubble "locating capture" and the control of bubble passing through or being blocked were achieved by using the laser-induced underwater superaerophilic/superaerophobic microstructures. The switchable underwater superaerophobic and superaerophilic surface may find broad applications in electrode reaction, antibubble

microfluidic devices and collecting useful or harmful gas in marine detecting.

4. Experimental Section

Femtosecond Laser Ablation: The femtosecond laser pulses were produced by a regenerative amplified Ti: sapphire laser system (Libra-usp-he, Coherent, America) with the central wavelength, pulse duration, and repetition rate of 800 nm, 50 fs, and 1 kHz, respectively. Figure 1a shows the setup of the femtosecond laser microfabrication system. The PTFE sheet (thickness of 1 mm) was fixed on a 3D translation platform controlled by a computer. The femtosecond laser beam was focused on the PTFE surface by an objective lens (20×, NA = 0.40, Nikon). Hierarchical rough microstructures were generated on the PTFE surface via the typical "line-by-line" laser scanning process at the laser power of 30 mW, the scanning speed of 5 mm s^{-1}, and the interval of scanning lines of 5 μm.

Vacuum-Pumping Treatment: The structured PTFE surface showed superhydrophobicity in air; thereby a trapped air layer formed in the surface microstructure after the immersion of the rough PTFE sample in water. To remove the trapped air layer around the laser-structured PTFE surface in a water medium, the underwater sample was treated by vacuumizing. The vacuum-pumping setup is shown in Figure 1b.

The sample was fixed on a holder and faced down. Then, the sample was immersed into water in a water reservoir. The whole reservoir was placed in a vacuum chamber and the system was vacuumed under the vacuum degree <10^4 Pa. This process lasted at least 10 min until scarcely any bubbles could be observed to escape from water. The trapped air was removed during this vacuumizing treatment, allowing the laser-ablated PTFE surface to switch from underwater superaerophilic to superaerophobic.

Fabrication of Through-Microhole-Structured Rough Sheet: The rough PTFE sheet with through-microholes array was fabricated by the mechanical drilling method and subsequent femtosecond laser ablation. The PTFE sheet with the thickness of 0.3 mm was drilled by a mini drill with the drill bit of 300 μm in diameter. The drill bit was controlled to pass through the PTFE sheet with the speed of 0.5 mm s^{-1}. The point-by-point drilling manner was used to form a microholes array and the center interval of the generated holes was set at 800 μm. After the formation of the microholes array, both sides of the PTFE sheet were further ablated by femtosecond laser to induce rough surface microstructures.

Characterization: A Quanta 250 FEG scanning electron microscope (FEI, America) was used to investigate the morphology of the femtosecond laser-structured PTFE surface. WCA, WSA, BCA, and bubble sliding angle were measured by a JC2000D contact-angle system (Powereach, China). All the values were measured at least three times, and had a margin of error of plus or minus 1.5°. The bubbles were pushed out from a bending microsyringe that was fixed below the sample in a homemade small water reservoir (Figure 1c). The dynamic movement of bubbles was recorded by a high-speed charge coupled device (CCD).

Acknowledgements

This work was supported by the National Key Research and Development Program of China under the Grant no. 2017YFB1104700, the National Science Foundation of China under the Grant nos. 51335008, 61875158, and 61805192, China Postdoctoral Science Foundation under the Grant no. 2016M600786, the Collaborative Innovation Center of Suzhou Nano Science and Technology. The SEM work was done at International Center for Dielectric Research (ICDR), Xi'an Jiaotong University.

Conflict of Interest

The authors declare no conflict of interest.

Keywords

air bubbles, femtosecond lasers, superhydrophobicity, underwater superaerophilicity, underwater superaerophobicity

Received: February 10, 2019
Revised: May 16, 2019
Published online: June 12, 2019

[1] C. Yu, P. Zhang, J. Wang, L. Jiang, *Adv. Mater.* **2017**, *29*, 1703053.
[2] J. George, S. Chidangil, S. George, *Adv. Mater. Interfaces* **2017**, *4*, 1601088.
[3] Z. Lu, W. Zhu, X. Yu, H. Zhang, Y. Li, X. Sun, X. Wang, H. Wang, J. Wang, J. Luo, X. Lei, L. Jiang, *Adv. Mater.* **2014**, *26*, 2683.
[4] B. Bhushan, Y. C. Jung, *Prog. Mater. Sci.* **2011**, *56*, 1.
[5] T. Ternes, M. Meisenheimer, D. Mcdowell, F. Sacher, H. Brauch, B. Gulde, G. Preuss, U. Wilme, N. Seibert, *Environ. Sci. Technol.* **2002**, *36*, 3855.
[6] M. Sarkar, S. Donne, G. Evans, *Adv. Powder Technol.* **2010**, *21*, 412.
[7] L. Yang, Y. Zhao, J. Yang, Y. Li, Q. Meng, *Water Sci. Technol.* **2014**, *70*, 627.
[8] P. Lv, Y. Xue, Y. Shi, H. Lin, H. Duan, *Phys. Rev. Lett.* **2014**, *112*, 196101.
[9] R. Yoon, *Int. J. Miner. Process.* **2000**, *58*, 129.
[10] Y. Gao, J. Li, H. C. Shum, H. Chen, *Langmuir* **2016**, *32*, 4815.
[11] M. Liu, S. Wang, L. Jiang, *Nat. Rev. Mater.* **2017**, *2*, 17036.
[12] Y. Tian, B. Su, L. Jiang, *Adv. Mater.* **2014**, *26*, 6872.
[13] M. Cao, L. Jiang, *Surf. Innovations* **2016**, *4*, 180.
[14] X. Chen, Y. Wu, B. Su, J. Wang, Y. Song, L. Jiang, *Adv. Mater.* **2012**, *24*, 5884.
[15] R. Seymour, P. Matthews, *J. Exp. Biol.* **2013**, *216*, 164.
[16] G. Wang, Y. Gao, S. Mitra, Y. Li, S. Zhou, G. Evans, *Int. J. Miner. Process.* **2015**, *142*, 22.
[17] G. Zhang, J. Schluter, X. Hu, *Ships Offshore Struct.* **2018**, *13*, 244.
[18] J. Chen, D. Chen, Y. Xie, X. Chen, K. Wang, D. Cui, H. Du, Z. Wang, *Appl. Phys. Lett.* **2015**, *106*, 053507.
[19] J. Wang, Y. Zheng, F. Nie, J. Zhai, L. Jiang, *Langmuir* **2009**, *25*, 14129.
[20] J. Yong, F. Chen, Y. Fang, J. Huo, Q. Yang, J. Zhang, H. Bian, X. Hou, *ACS Appl. Mater. Interfaces* **2017**, *9*, 39863.
[21] J. Yong, F. Chen, J. Huo, Y. Fang, Q. Yang, J. Zhang, X. Hou, *Nanoscale* **2018**, *10*, 3688.
[22] J. Yong, F. Chen, W. Li, J. Huo, Y. Fang, Q. Yang, H. Bian, X. Hou, *Global Challenges* **2018**, *2*, 1700133.
[23] Y. Lei, R. Sun, X. Zhang, X. Feng, L. Jiang, *Adv. Mater.* **2016**, *28*, 1477.
[24] C. Shi, X. Cui, X. Zhang, P. Tchoukov, Q. Liu, N. Encinas, M. Paven, F. Geyer, D. Vollmer, Z. Xu, H. Butt, H. Zeng, *Langmuir* **2015**, *31*, 7317.
[25] J. Ming, Q. Yang, M. Wang, C. Wang, L. Jiang, *Soft Matter* **2012**, *8*, 2261.
[26] Z. Lu, M. Sun, T. Xu, Y. Li, W. Xu, Z. Chang, Y. Ding, X. Sun, L. Jiang, *Adv. Mater.* **2015**, *27*, 2361.
[27] W. Xu, Z. Lu, P. Wan, Y. Kuang, X. Sun, *Small* **2016**, *12*, 2492.
[28] J. L. Yong, S. C. Singh, Z. Zhan, F. Chen, C. Guo, *ACS Appl. Mater. Interfaces* **2019**, *11*, 8667.
[29] J. L. Yong, S. C. Singh, Z. Zhan, F. Chen, C. Guo, *Langmuir* **2019**, *35*, 921.
[30] C. Dorrer, J. Ruhe, *Langmuir* **2012**, *28*, 14968.

[31] H. Yang, J. Hou, L. Wan, V. Chen, Z. Xu, *Adv. Mater. Interfaces* **2016**, *3*, 1500774.
[32] Z. Lu, Y. Li, X. Lei, J. Liu, X. Sun, *Mater. Horiz.* **2015**, *2*, 294.
[33] J. Wang, Y. Liu, Y. Zhang, J. Feng, H. Wang, Y. Yu, H. Sun, *Adv. Funct. Mater.* **2018**, *28*, 1800625.
[34] Y. Fang, J. Yong, F. Chen, J. Huo, Q. Yang, H. Bian, G. Du, X. Hou, *Appl. Phys. A* **2016**, *122*, 827.
[35] J. Yong, Y. Fang, F. Chen, J. Huo, Q. Yang, H. Bian, G. Du, X. Hou, *Appl. Surf. Sci.* **2016**, *389*, 1148.
[36] J. Yong, J. Huo, Q. Yang, F. Chen, Y. Fang, X. Wu, L. Liu, J. Zhang, X. Hou, *Adv. Mater. Interfaces* **2018**, *5*, 1701479.
[37] J. Yong, F. Chen, Q. Yang, J. Zhang, X. Hou, *Adv. Mater. Interfaces* **2018**, *5*, 1701370.
[38] Y. Chen, Y. Zhang, L. Shi, J. Li, Y. Xin, T. Yang, Z. Guo, *Appl. Phys. Lett.* **2012**, *101*, 033701.
[39] H. Wu, Z. Yang, B. Caom, Z. Zhang, K. Zhu, B. Wu, S. Jiang, G. Chai, *Langmuir* **2017**, *33*, 407.
[40] A. Marmur, *Langmuir* **2003**, *19*, 8343.

